

# RSC Advances



This is an *Accepted Manuscript*, which has been through the Royal Society of Chemistry peer review process and has been accepted for publication.

*Accepted Manuscripts* are published online shortly after acceptance, before technical editing, formatting and proof reading. Using this free service, authors can make their results available to the community, in citable form, before we publish the edited article. This *Accepted Manuscript* will be replaced by the edited, formatted and paginated article as soon as this is available.

You can find more information about *Accepted Manuscripts* in the [Information for Authors](#).

Please note that technical editing may introduce minor changes to the text and/or graphics, which may alter content. The journal's standard [Terms & Conditions](#) and the [Ethical guidelines](#) still apply. In no event shall the Royal Society of Chemistry be held responsible for any errors or omissions in this *Accepted Manuscript* or any consequences arising from the use of any information it contains.

1

2 **Modelling the effects of surfactant loading level on the sorption of**  
3 **organic contaminants on organoclays**

4 Qing Zhou<sup>1,2,3</sup>, Runliang Zhu<sup>1,2\*</sup>, Stephen C. Parker<sup>4\*</sup>, Jianxi Zhu<sup>1,2</sup>, Hongping He<sup>1,2</sup>,

5 Marco Molinari<sup>4</sup>

6 <sup>1</sup> *Key laboratory of Mineralogy and Metallogeny, Guangzhou Institute of Geochemistry, Chinese*  
7 *Academy of Sciences, Guangzhou 510640, China*

8 <sup>2</sup> *Guangdong Provincial Key Laboratory of Mineral Physics and Material Research & Development,*  
9 *Guangzhou 510640, China*

10 <sup>3</sup> *University of Chinese Academy of Sciences, Beijing 100049, China*

11 <sup>4</sup> *Department of Chemistry, University of Bath, Claverton Down, Bath BA2 7AY, U.K.*

12

13 \* Corresponding author 1

14 Phone: 86-020-85297603

15 Fax: 86-020-85297603

16 E-mail: zhurl@gig.ac.cn

17

18 \* Corresponding author 2

19 Phone: +44 (0) 1225 386505

20 Fax: +44 (0) 1225 386231

21 E-mail: S.C.Parker@bath.ac.uk

22

---

**23 Abstract**

24 Organoclays can effectively uptake organic contaminants (OCs) from water media,  
25 but the sorption mechanisms are not fully established yet, because of the lack of  
26 recognition of interlayer structure of organoclays. To unravel this complex behavior,  
27 we have examined the effects of surfactant loading on the interlayer structure and  
28 sorption behaviors of organoclays using molecular dynamics (MD) simulations. The  
29 sorption behavior of phenol on three cetyltrimethylammonium intercalated  
30 montmorillonite (CTMA-Mt) with CTMA loading levels of 0.33, 1.0, and 1.66 times  
31 of the Mt's cation exchange capacity (CEC), was studied. The results demonstrated  
32 that CTMA aggregates were the main sorption domains for phenol molecules,  
33 consistent with a partition process. The interlayer structure of CTMA-Mt influences  
34 the sorption affinity of phenol. CTMA aggregates increased in size with increasing  
35 loading level, creating larger sorption domains for phenol uptake. On the other hand,  
36 high CTMA loading level decreased the sorption affinity of CTMA-Mt (with 1.66  
37 CEC loading) toward phenol by increasing the packing density and cohesive  
38 characteristic of the aggregates. In addition, the siloxane surfaces of Mt and the  
39 hydrated inorganic ions ( $\text{Ca}^{2+}$  or  $\text{Br}^-$ ) showed specific interactions with phenol  
40 molecules by forming H-bond. The oxygen atoms on siloxane surface and water  
41 molecules around  $\text{Br}^-$  serve as H-bond acceptor while water molecules around  $\text{Ca}^{2+}$   
42 serve as H-bond donor, corresponding to polyparameter linear free energy  
43 relationships (pp-LFERs) results. The modelling results correlate well with the  
44 experimental findings, and further reveal that the sorption affinity strongly depends on  
45 the size and packing density of surfactant aggregates. In addition, H-bond interactions  
46 should be considered as well in the sorption of OCs containing particular groups.

47 **Keywords:** Organoclays; Cationic surfactant; Sorption; Organic contaminants;

---

48 Montmorillonite; Pollutants, Molecular dynamics

---

## 49 Introduction

50 Organoclays are synthesized by exchanging the interlayer inorganic cations using  
51 cationic surfactants (e.g. cetyltrimethylammonium (CTMA)), to effectively and  
52 efficiently uptake organic contaminants (OCs) from aqueous media.<sup>1-9</sup> However, the  
53 sorption mechanisms underlying the uptake process have not been unambiguously  
54 clarified yet. Early studies indicated that the sorption of OCs was primarily a partition  
55 process, i.e., partition of OCs between bulk water and the organic phases formed by  
56 surfactant aggregates in organoclays.<sup>3-6</sup> More recent studies, however, have shown  
57 that the sorption mechanism is not just a simple partition process as the organic  
58 carbon-normalized sorption coefficient ( $K_{oc}$ ) of a given OC varies over one order of  
59 magnitude on different organoclays.<sup>6-18</sup> Thus, the sorption results from the change in  
60 the microstructure of the organoclays, which depends on an intricate play between  
61 different depending on factors such as charge type and density of clay minerals,<sup>8-14</sup>  
62 molecular structure and loading level of cationic surfactants.<sup>5, 6, 13-21</sup>

63 Of particular interest is the effect of surfactant loading on  $K_{oc}$ .  $K_{oc}$  for a given OC  
64 often shows an evolution trend that first increases and then decreases with increasing  
65 surfactant loading level, with the maximum value generally appearing at  $\sim 1.0$  times of  
66 the cation exchange capacity (CEC) of the clay minerals.<sup>13-19, 22</sup> To explain this  
67 curious change in sorption behavior various hypothesis have been proposed. Bonczek  
68 *et al.*<sup>22</sup> proposed that organoclays with larger basal spacing have greater interlayer  
69 accessibility for OCs, while Chen *et al.*<sup>16</sup> suggested that the intercalated cationic  
70 surfactant forms adsorptive films with high affinity toward OCs at relatively low  
71 loading level and bulk organic phases with weak affinity toward OCs at high loading  
72 level. Bartelt-Hunt *et al.*<sup>18</sup> and Zhu *et al.*<sup>13, 14</sup> proposed a change in the microstructure  
73 of the surfactant aggregates at different loading level, which leads to a different

74 sorption affinity toward OCs, while Xu *et al.*<sup>19</sup> and Bonczek *et al.*<sup>22</sup> suggested that the  
75 hydration of interlayer inorganic ions decreases the hydrophobicity of the interlayer  
76 space, which leads to a decrease of  $K_{oc}$ . These wide range of explanations can be  
77 attributed to the structure of the interlayer, which is rather complex (e.g. arrangement  
78 of intercalated surfactant, solvent molecules, and intercalated ions) and can hardly be  
79 characterized by experimental techniques, particularly in an aqueous environment.

80 Molecular modelling is an efficient method for understanding the interlayer  
81 structure of clay minerals and organoclays by giving atom-level insights into  
82 structural features and transport properties.<sup>23-29</sup> Zhao and Burns<sup>32, 33</sup> and Zhu *et al.*<sup>30</sup>  
83 showed that OCs molecules were primarily sorbed within CTMA aggregates. Shapley  
84 *et al.*<sup>34</sup> calculated a negative free energy for the sorption of polychlorinated  
85 dibenzo-p-dioxins (PCDDs) from bulk water into the interlayer space of CTMA-Mt,  
86 finding that intercalated CTMA creates a hydrophobic environment for the sorption of  
87 PCDDs. These molecular modelling studies further proved the sorption of OCs on  
88 organoclays is primarily a partition process.

89 Although, the modelling research has laid the foundations to understand the  
90 atom-level interaction between OCs and CTMA-Mt, the experimental observations  
91 are still not fully understood and the effect of surfactant loading on the sorption of  
92 OCs remains unexplained. Thus, this work explores the effects of surfactant loading  
93 on the interlayer structure and sorption behaviors of organoclay CTMA-Mt using MD  
94 simulations, to provide fundamental understanding of the experimental findings and  
95 in general on the sorption mechanisms of OCs in organoclays.

96

## 97 MATERIALS AND METHODS

98 **Models.** Mt model with chemical formula  $\text{Ca}_{0.375}[\text{Al}_{3.25}\text{Mg}_{0.75}][\text{Si}_8] \text{O}_{20}(\text{OH})_4$  was

99 used as in previous studies.<sup>28</sup> In this model, the isomorphic substitutions obey  
100 Loewenstein's rule.<sup>35</sup> The simulation cell has dimensions of 20.80 Å × 36.02 Å ×  
101 variable Å, comprising of two layers of 16 unit cells of montmorillonite (4x × 4y × 1z  
102 expansion). The surfactant cetyltrimethylammonium (CTMA) was chosen to allow for  
103 comparison with previous studies.<sup>13, 17, 28, 30</sup> 4, 12, 20 CTMA ions, representing three  
104 loading levels of CTMA, i.e., 0.33, 1.00, and 1.66 times of Mt's CEC, were  
105 intercalated into the Mt interlayer to study the effect of the loading on the structure of  
106 the interlayer. For 0.33 CTMA loading, 4 Ca<sup>2+</sup> ions were added to the interlayer, while  
107 for 1.66 CTMA loading, 8 Br<sup>-</sup> ions were added to maintain overall charge neutrality of  
108 the simulation cell. To model the water saturated conditions, water molecules were  
109 gradually added (50 molecules at each step) into the interlayer of CTMA-Mt, until the  
110 basal spacing value was close to experimental  $d_{001}$  values of wet samples (28.2 Å for  
111 0.33 CTMA loading, 30.5 Å for 1.00 CTMA loading, 36.5 Å for 1.66 CTMA  
112 loading).<sup>28, 30</sup> Finally, the water amount for 0.33, 1.0 and 1.66 CTMA loading was 400,  
113 300, 300 respectively. Phenol was selected as representative of OCs as it has both  
114 nonspecific van der Waals interaction and specific H-bond interaction with CTMA-Mt  
115 and water.<sup>30</sup> Experiments showed that the adsorption amount of phenol is about 12.3  
116 mg/g of sorbed concentration, corresponding to 4.24 phenol molecules in our  
117 simulation system.<sup>30</sup> In addition, adsorption of phenol did not cause the increase of  
118 basal spacing of CTMA-Mt, indicating that some of the water molecules left the  
119 interlayer space during the sorption process. To clarify the exact number of water  
120 molecules replaced by phenol, a series of test modelling have been performed by  
121 increasing the water / phenol ratio from 3 to 6. The results showed that when 4 water  
122 were replaced by 1 phenol, the basal spacing values remained constant.<sup>30</sup> Therefore,  
123 the sorption of phenol into water saturated CTMA-Mt was modeled by adding 4

124 phenol molecules randomly into the interlayer while 16 water molecules were  
125 removed.

126 **Molecular modelling methods.** MD simulations were undertaken using the  
127 DL\_POLY code (version 2.20).<sup>36</sup> Classical potential modelling based on the Born  
128 model description of the ionic lattice assumes the interaction forces between ions  
129 consist of a long-range Coulombic term and a short-range potential. The equations of  
130 motion were updated using the Verlet-Leapfrog algorithm and the Ewald method was  
131 used for evaluating the electrostatic interactions. A short range potential cutoff of 9.5  
132 Å was used and three dimensional periodic boundary conditions were applied.

133 CLAYFF force field was applied to simulate the system.<sup>37</sup> CLAYFF has been  
134 widely and successfully used for modelling clay minerals and organoclays.<sup>23-34</sup> In this  
135 force field, the interactions between the atomic species are described by  
136 Lennard-Jones parameters and Coulombic terms with partial charge, while hydroxyl  
137 groups (OH) are described by a harmonic term. The water solvent was represented by  
138 using the single point charge (SPC) water model as implemented within CLAYFF.<sup>37, 38</sup>  
139 The CVFF force field was used to represent CTMA and phenol.<sup>39</sup> CVFF has been  
140 successfully used in the simulations of mineral-organic interfaces and  
141 alkylammonium intercalated Mt.<sup>28-30</sup> The strength of this combination of force field is  
142 that all use Lennard-Jones parameters and partial charges that can be mixed by using  
143 simple mixing rules.<sup>37</sup>

144 We applied a geometry optimization to each simulation cell first to obtain the  
145 minimum energy structure, which ensured a faster equilibration. Then, NPT (300 K, 1  
146 atm) simulations were performed for 3 ns to achieve equilibrium, and another 1 ns to  
147 record the basal spacings. When systems reach equilibrium, the volume was fixed and  
148 a further 3 ns NVT (300 K) simulations and data collection were performed. In all



149 simulations the time step was set to 1.0 fs and all atoms were allowed to move.

150 Through post-analysis of the MD trajectories, 2D-density profiles, z-densities,  
151 radial distribution function (RDF), average H-bond number, self-diffusion coefficients  
152 and occupied volume of CTMA cations were analyzed as previously described.<sup>34, 40, 41</sup>  
153 The 2D-density profile is the 2 dimensional time-averaged (over the duration of the  
154 simulation) density plots which give qualitative information not only about how dense  
155 the CTMA and phenol in the interlayer but also the favored adsorption sites. The  
156 z-density was calculated dividing the system into slices of 0.3 Å along the z direction.  
157 The H-bond between phenol and water molecules was determined by imposing two  
158 conditions: (1) a distance between the donor and acceptor smaller than 3 Å; (2) a  
159 H-O...O angle smaller than 30°. <sup>42</sup> The packing density was evaluated from the mass  
160 divided by the occupied volume of CTMA cations. The occupied volume of CTMA  
161 cations was calculated by subtracting the occupied volume of other interlayer species  
162 (including water, phenol, Ca<sup>2+</sup> and Br<sup>-</sup>) from the interlayer spaces, and then the  
163 packing densities of CTMA aggregates was further calculated. The height of the  
164 interlayer space was determined considering the van der Waals radius of siloxane  
165 surface. Though the density of water varies with different interlayer spacing because  
166 of the confining effect of Mt layer, previous simulations have shown that the change  
167 of water density in the interlayer of water saturated CTMA-Mt with increasing  
168 loading level is negligible and the density mainly based on the chosen water potential  
169 model.<sup>28</sup> So the volume of single water molecule was 0.0297 nm<sup>3</sup> basing on the SPC  
170 water model.<sup>38</sup> Phenol was calculated to be 0.1458 nm<sup>3</sup> basing on a NPT ensemble  
171 simulation of 1500 water and 4 phenol under same P-T conditions. The volume of  
172 Ca<sup>2+</sup> and Br<sup>-</sup> was 0.0042 nm<sup>3</sup> and 0.0315 nm<sup>3</sup> basing on their ion radii.

173 **RESULTS AND DISCUSSION**

---

## 174 1. Arrangement of the interlayer species

175 The snapshots, 2D density profiles of CTMA carbon on the alkyl chain (C3)  
176 and phenol carbon (CR), and Z-density profiles of the interlayer species of  
177 0.33CTMA-Mt, 1.0CTMA-Mt, and 1.66CTMA-Mt were compared (Figure 1). The  
178 results showed that the charged head groups of CTMA cations were directly attached  
179 to the siloxane surface, although the head groups are not tethered to the surface, which  
180 could be attributed to the electrostatic interactions between the positively-charged  
181 head groups and the negatively charged siloxane surface.<sup>28, 30</sup> The alkyl chains tended  
182 to either adsorb onto the siloxane surface or extend into the interlayer space forming  
183 alkyl chain aggregates. The loading level of CTMA affected the size of the CTMA  
184 aggregates. At low loading level (i.e., 0.33CTMA-Mt), a large portion of the alkyl  
185 chains adsorbed onto the siloxane surface while only a small amount extended into  
186 the interlayer space to form aggregates (Figure 1a). With increasing CTMA loading  
187 level, more alkyl chains extended in the interlayer space to form aggregates, and  
188 accordingly the size of CTMA aggregates increased. In 1.66CTMA-Mt, the CTMA  
189 loading exceeded the cation exchange capacity of Mt, causing Br<sup>-</sup> enter the interlayer  
190 space as counter ions. Some bromine ions resulted trapped into the aggregates. This  
191 caused the head groups of the extra CTMA (together with interlayer water molecules)  
192 to re-locate in the middle of the interlayer space, while their alkyl chains stretched  
193 away to form aggregates with CTMA cations (Figure 1c). This is again related to the  
194 electrostatic interaction within to oppositely charged groups.

195 The transport properties of CTMA were investigated by calculating the  
196 self-diffusion coefficients of C3 (CTMA carbon on the alkyl chain). It was found that  
197  $D_{C3}$  decreased with CTMA loading level (Table 1). The low mobility of CTMA at its  
198 high loading level arises from the high packing density. Although several

199 experimental studies suggested that the packing density of CTMA should increase  
200 with loading level, this work for the first time accurately calculated the packing  
201 density of CTMA aggregates on water-saturated CTMA-Mt, which was shown to  
202 increase with increasing loading level (Table 1). Thus, this work clearly shows that  
203 the packing density of CTMA increased with its loading level, indicating indeed that  
204 the interlayer microstructure changes radically depending on the CTMA loading level.

205 When phenol was present in the interlayer, it was mainly located within the  
206 CTMA aggregates on 1.0CTMA-Mt and 1.66CTMA-Mt (Figure 1b and c), which  
207 suggested a partition mechanism for uptaking phenol, consistent with previous  
208 experimental and modelling results.<sup>9-15, 30-34</sup> On the other hand, as the size of CTMA  
209 aggregate on 0.33CTMA-Mt was rather small, some of the phenol molecules were  
210 sorbed on the surface of the CTMA aggregate (Figure 1a). This indicates that at low  
211 CTMA loading level, the surfactant was unable to form large aggregates which are  
212 likely responsible for phenol uptake. The transport properties of phenol were also  
213 investigated by calculating the self-diffusion coefficients of CP (phenol carbon)  
214 (Table 1). Phenol showed higher mobility in 0.33CTMA-Mt, but similar lower  
215 mobility in 1.0CTMA-Mt and 1.66CTMA-Mt, indicating the confining effect from  
216 CTMA aggregates, in accordance with 2D density profile (Figure 1). Thus, we infer  
217 that as the structure of the nano-sized surfactant aggregates changes with surfactant  
218 loading level, their interactions with OCs will be affected to a different extent.  
219 Besides the organic cations, the siloxane surface also contribute to the sorption of  
220 phenol molecules. Phenol indeed could be sorbed on the siloxane surface through the  
221 -OH group as the oxygen atoms of the siloxane surface could act as H-bond  
222 acceptor.<sup>30</sup>

223 Although the arrangement of interlayer cations in montmorillonite has been

224 reported by previous studies, the distribution of interlayer cations and anions in water  
225 saturated organoclays was not well discussed. Our modelling results showed that  $\text{Ca}^{2+}$   
226 cations on 0.33CTMA-Mt mainly located close to the siloxane surface (Figure 1a),  
227 which is attributed to the electrostatic interactions between them. According to the  
228 snapshot and Z-density profiles,  $\text{Ca}^{2+}$  cations resided on the siloxane surface,  
229 similarly to previous modelling study on montmorillonite without intercalated organic  
230 cations.<sup>27</sup> From the RDF profiles of Ca-OW (water oxygen) and Ca-HC (CTMA  
231 hydrogen), the coordination number of water molecules surrounding  $\text{Ca}^{2+}$  cations was  
232 calculated to be 7-8 water molecules, indicating that there is no direct interaction  
233 between  $\text{Ca}^{2+}$  and CTMA molecules (Figure 2a). On the other hand,  $\text{Br}^-$  anions on  
234 1.66CTMA-Mt, almost completely located in the middle of interlayer space, i.e.,  
235 away from the siloxane surface (Figure 1c), which is attributed to the electrostatic  
236 interaction between  $\text{Br}^-$  and the head group of CTMA, and the electrostatic repulsion  
237 between  $\text{Br}^-$  and negatively charged siloxane surface as well. The RDF profiles of  
238 Br-HW and Br-HC (Figure 2b) indicated that hydrated  $\text{Br}^-$  does not directly interact  
239 with CTMA as well. However, the RDF of Br-NC (CTMA nitrogen) reveals the  
240 bonding of hydrated  $\text{Br}^-$  anions to the charged head group of CTMA (Figure 2b).

241 Within the interlayer spaces of 1.0CTMA-Mt and 1.66CTMA-Mt, water  
242 molecules were shown to mostly occupy the spaces between CTMA aggregates  
243 (Figure 1b, c). As for 0.33CTMA-Mt, water molecules occupied a large portion of the  
244 interlayer space, and some water molecules could even penetrate into the loosely  
245 associated CTMA aggregates (Figure 1a). On the other hand, the Z-density profiles  
246 showed that water molecules had high density above the siloxane surface for all the  
247 three samples, which could be attributed to the hydration of the siloxane surface and  
248 the formation of H-bonds.<sup>26-30, 43-46</sup>

---

## 249 2. Effects of inorganic ions on the sorption of phenol molecules

250 Although several experimental studies have proposed that inorganic ions affect  
251 the sorption of OCs on organoclays,<sup>19,22</sup> modelling studies are still lacking. Xu et al.<sup>19</sup>  
252 suggested that the hydration of the inorganic ions decreases the hydrophobicity of the  
253 interlayer spaces, leading to weaker sorption capacity of the organoclays. However,  
254 no direct structural evidences were presented, as the experimental techniques can  
255 hardly provide high resolution information of the arrangement and hydration of  
256 inorganic ions in water saturated organoclays.

257 Our results demonstrated that the hydrated inorganic ions ( $\text{Ca}^{2+}$  and  $\text{Br}^-$ ) were  
258 mainly located in the water solvent and generally would not be incorporated into the  
259 CTMA aggregates and the uptake of phenol is partition process. As such, one might  
260 expect the influence of the hydrated inorganic ions on the partition behaviors of the  
261 CTMA aggregates would be less than the bulk water case. However, it is worth noting  
262 that the nano-sized surfactant aggregates have large interface with the interlayer water,  
263 and it is likely that some of the OCs would be sorbed at/near this interface. In this  
264 instance, the inorganic ions affect the sorption of OCs on organoclays. As water  
265 molecules surrounding  $\text{Ca}^{2+}$  showed particular orientation, i.e., with OW (water  
266 oxygen) pointing towards  $\text{Ca}^{2+}$  (Figure 3a and 4a), they tend to act as H-bond donor  
267 and then will help the sorption of OCs with H-bond acceptor capability. On the other  
268 hand, water molecules surrounding  $\text{Br}^-$  had reverse orientation (Figure 3b and 4b), and  
269 then they will help the sorption of OCs with H-bond donor capability.

270 The  $-\text{OH}$  group on phenol molecule can be both H-bond donor and acceptor.<sup>47</sup> If  
271 the inorganic ions can affect the sorption of phenol on organoclays, the orientation of  
272  $-\text{OH}$  group surrounding the inorganic ions (i.e.,  $\text{Ca}^{2+}$  or  $\text{Br}^-$ ) should be quite different.  
273 To address these points, we present the RDF between the phenol and the inorganic

274 cations. The RDF profiles of Ca-OP (–OH oxygen on phenol), Ca-HP (–OH hydrogen  
275 on phenol), Br-OP, and Br-HP were compared in Figure 3c and 3d and showed that Ca  
276 ions interacted more strongly with the OP while the Br<sup>–</sup> ions with the HP, consistent  
277 with our hypothesis. Interestingly, the RDFs clearly showed that phenol interacts only  
278 with the hydration shell of Ca<sup>2+</sup> while it interacts directly with Br<sup>–</sup>. Direct interactions  
279 between OCs with inorganic ions were also reported in previous studies, particularly  
280 for the ions with relatively weak hydration capacity such as Cs and K.<sup>48-50</sup> The  
281 hydration enthalpy of Br<sup>–</sup> is indeed -328 kJ/mol, close to that of K<sup>+</sup> (-340 kJ/mol), but  
282 much smaller than that of Ca<sup>2+</sup> (-1616 kJ/mol).<sup>51</sup> It is worth noting that one may  
283 expect that when anions with stronger hydration capacity (e.g., F<sup>–</sup>, -504 kJ/mol)<sup>51</sup> are  
284 presented in the interlayer, phenol may interact with the hydration shell instead of the  
285 anion. This is clearly not the case in this study.

286 The snapshots of 0.33CTMA-Mt and 1.66CTMA-Mt after removing CTMA  
287 were plotted to show the interlayer H-bond network (Figure 4). Water molecules  
288 around inorganic ions showed special orientation, i.e., with OW pointing toward Ca<sup>2+</sup>  
289 on 0.33CTMA-Mt while HW pointing toward Br<sup>–</sup> on 1.66CTMA-Mt. As a result,  
290 water molecules around Ca<sup>2+</sup> could be H-bond donor when interacting with phenol  
291 molecules (Figure 4a), while those around Br<sup>–</sup> tended to be H-bond acceptor (Figure  
292 4b). Moreover, phenol may also penetrate the hydration shell and directly interact  
293 with Br<sup>–</sup>.

294 The average numbers of H-bond formed between water molecules and each  
295 phenol molecule were calculated (Table 1). One should notice that phenol molecules  
296 on all the three samples were more likely to be H-bond donor (D) rather than acceptor  
297 (A) when forming H-bond with water molecules, which should be attributed to its  
298 physicochemical properties, i.e., stronger ability to be H-bond donor than acceptor.<sup>48</sup>

299 With increasing CTMA loading level, the total number of H-bonds for each phenol  
300 molecules decreased drastically, which is consistent with the phenol molecules being  
301 located within the CTMA aggregates (as the aggregates became larger). In addition,  
302 the numbers of D type H-bond did not change much with increasing CTMA loading  
303 level, while those of A type decreased drastically. As a result, the ratio of D/A  
304 increased significantly with increasing CTMA loading level, which again proved that  
305 the hydrated inorganic ions can evidently affect the formation of H-bond between  
306 phenol and water molecules. However, one should also notice that the number of  
307 H-bonds formed between water and phenol molecules on CTMA-Mt was smaller than  
308 those in bulk water ( $\sim 0.78$  H-bond on average according to our calculation), which is  
309 consistent with the fact that phenol molecules were mainly located in the CTMA  
310 aggregates.

### 311 **3. Comparison with previous experimental studies**

312 Combining the modelling results of this work with previous experimental studies  
313 provides novel insights for clarifying the sorptive characteristics of organoclays. Zhu  
314 *et al.*<sup>52</sup> studied the effects of surfactant loading level on the sorption thermodynamics  
315 of CTMA-Mt toward naphthalene, showing that the sorption process was primarily  
316 driven by the entropy term, while the enthalpy term showed positive contribution at  
317 low CTMA loading level (i.e.,  $\sim 0.2$  CEC and  $\sim 1.0$  CEC) and negative contribution at  
318 high loading level ( $\sim 1.8$  CEC). The sorption enthalpy of naphthalene was notably less  
319 exothermic than the desolvation enthalpy of naphthalene, which confirmed a partition  
320 into the CTMA aggregates rather than a condensation on the surface of CTMA-Mt,  
321 well in agreement with the modeling results of this study. Combining the  
322 characterization results and the calculated thermodynamic values, they further  
323 proposed that CTMA within the interlayer of CTMA-Mt could form various organic

324 phases for the sorption of OCs as the loading level changed.<sup>52</sup> Our modelling results  
325 clearly demonstrated the CTMA aggregates change in size and packing density with  
326 increasing CTMA loading level, not only consistent with their proposal, but also  
327 reveals the microstructure of CTMA aggregates at atomic level.

328 Recently, Zhu *et al.*<sup>52</sup> studied the effect of CTMA loading level (0.4CEC,  
329 1.0CEC, and 1.6CEC) on the sorptive characteristics of CTMA-Mt using  
330 polyparameter linear free energy relationships (pp-LFERs) analysis, which directly  
331 show the relative contributions of individual intermolecular interactions to a sorption  
332 process.<sup>53-56</sup> Their results demonstrated that the driving forces for the sorption of OCs  
333 in CTMA-Mt arise from weaker cohesive characteristics, stronger dispersion  
334 interaction and H-bond acceptor capacity, compared to bulk water. On the other hand,  
335 CTMA-Mt showed weaker polar/polarization interaction and H-bond donor capacity,  
336 which had a negative contribution to the sorption process. These results suggested that  
337 the OCs should be primarily sorbed into organic phases (i.e., CTMA aggregates),  
338 consistent with the modelling results of this work as well. The strong H-bond acceptor  
339 capacity was suggested to rise from the oxygen atoms on the siloxane surfaces, which  
340 could accept hydrogen atoms to form H-bond in our modelling results.

341 With increasing CTMA loading level, they further showed that the CTMA-Mt  
342 became more cohesive with stronger polarization interaction and H-bond acceptor  
343 capacity, but weaker H-bond donor capacity, also shown in our modelling results. As  
344 the size of CTMA aggregates became larger, OCs were more likely to be sorbed  
345 within the aggregates rather than at their surface, which then caused stronger  
346 dispersion interaction between CTMA-Mt and OCs. As is well known, OCs generally  
347 have stronger dispersion interaction with organic phases than with water molecules  
348 (i.e., easier to form a cavity for the accommodation of OCs molecule).<sup>30, 53, 54</sup> More



349 cohesive characteristics of CTMA-Mt with higher CTMA loading should be caused  
350 by the larger packing density of CTMA aggregates, as in this case creating a cavity  
351 within the aggregates should consume more free energy. As the interlayer inorganic  
352 ions changed from cations to anions, the interlayer water molecules then behaved  
353 more likely as H-bond donor than acceptor, which then weakened the H-bond donor  
354 capacity of the resulting CTMA-Mt. As such, our modelling results correlated with  
355 previous pp-LFERs studies well, and gave atom-level insight to explain the  
356 macroscopic sorption property (i.e. uptake of OCs) of CTMA-Mt depending on the  
357 CTMA loading level.

### 358 **Conclusions**

359 In summary, molecular modelling gave atom-level insight into the interlayer  
360 structure of CTMA-Mt by showing the arrangement of interlayer species. Our results  
361 provided additional information supporting that the sorption of OCs on organoclays is  
362 a partition controlled process, and OCs molecules are mainly sorbed into surfactant  
363 aggregates (i.e., organic phases). Our results clearly demonstrated that the loading  
364 level of surfactant significantly affect the structure of the aggregates (e.g., size,  
365 packing density, etc.), and accordingly their sorption affinity towards OCs. In addition,  
366 siloxane surface and interlayer inorganic ions have specific interactions with OCs,  
367 particularly those containing H-bond acceptor/donor capabilities, which then can have  
368 additional effects to the sorption behaviors of organoclays.

369

### 370 **ACKNOWLEDGEMENT**

371 This work was financially supported by the “One Hundred Talents program” of the  
372 Chinese Academy of Sciences (KZZD-EW-TZ-10), grants from the National Natural  
373 Science Foundation of China (41322014, 21177104), the Royal Society BP Amoco

374 Research Fellowship (RC-H1054), and CAS/SAFEA International Partnership  
375 Program for Creative Research Teams (20140491534). Dr Molinari and Prof. Parker  
376 would like to acknowledge the EPSRC for funding (EP/I03601X/1) and the Materials  
377 Chemistry Consortium funded by EPSRC (EP/L000202) for access to the ARCHER  
378 facility.

379

## 380 REFERENCES

- 381 (1) Park, Y.; Ayoko, G. A.; Frost, R. L. Application of organoclays for the adsorption of recalcitrant  
382 organic molecules from aqueous media. *J. Colloid Interface Sci.* **2011**, *354* (1), 292–305.
- 383 (2) Fatimah, I.; Huda, T. Preparation of cetyltrimethylammonium intercalated Indonesian  
384 montmorillonite for adsorption of toluene. *Appl. Clay Sci.* **2013**, *74*, 115–120.
- 385 (3) Boyd, S. A.; Mortland, M. M.; Chiou, C. T. Sorption characteristics of organic-compounds on  
386 hexadecyltrimethylammonium-smectite. *Soil Sci. Soc. Am. J.* **1988**, *52* (3), 652–657.
- 387 (4) Boyd, S. A.; Shaobai, S.; Lee, J. F.; Mortland, M. M. Pentachlorophenol sorption by  
388 organo-clays. *Clays Clay Miner.* **1988**, *36* (2), 125–130.
- 389 (5) Smith, J. A.; Jaffe, P. R.; Chiou, C. T. Effect of 10 quaternary ammonium cations on  
390 tetrachloromethane sorption to clay from water. *Environ. Sci. Technol.* **1990**, *24* (8), 1167–1172.
- 391 (6) Smith, J. A.; Galan, A. Sorption of nonionic organic contaminants to single and dual organic  
392 cation bentonites from water. *Environ. Sci. Technol.* **1995**, *29* (3), 685–692.
- 393 (7) Zhu, L.; Li, Y.; Zhang, J. Sorption of organobentonites to some organic pollutants in water.  
394 *Environ. Sci. Technol.* **1997**, *31* (5), 1407–1410.
- 395 (8) Yuan, G. D.; Theng, B. K. G.; Churchman, G. J.; Gates, W. P. Clays and clay minerals for  
396 pollution control. In *Handbook of Clay Science*, 2<sup>nd</sup> ed.; Bergaya, F., Lagaly, G., Eds.; Elsevier:  
397 Amsterdam 2013; pp 587–644.
- 398 (9) Slade, P. G.; Gates, W. P. The swelling of HDTMA smectites as influenced by their preparation  
399 and layer charges. *Appl. Clay Sci.* **2004**, *25* (1–2), 93–101.
- 400 (10) Jaynes, W. F.; Boyd, S. A. Clay mineral type and organic-compound sorption by  
401 hexadecyltrimethylammonium-exchanged clays. *Soil Sci. Soc. Am. J.* **1991**, *55* (1), 43–48.
- 402 (11) Sheng, G. Y.; Xu, S. H.; Boyd, S. A. Mechanism(s) controlling sorption of neutral organic  
403 contaminants by surfactant-derived and natural organic matter. *Environ. Sci. Technol.* **1996**, *30* (5),  
404 1553–1557.
- 405 (12) Shen, Y. H. Phenol sorption by organoclays having different charge characteristics. *Colloids*  
406 *Surface, A.* **2004**, *232* (2–3), 143–149.
- 407 (13) Zhu, R.; Zhu, L.; Xu, L. Sorption characteristics of CTMA-bentonite complexes as controlled  
408 by surfactant packing density. *Colloids Surface, A.* **2007**, *294* (1–3), 221–227.
- 409 (14) Zhu, R.; Zhu, L.; Zhu, J.; Xu, L. Structure of surfactant-clay complexes and their sorptive  
410 characteristics toward HOCs. *Sep. Purif. Technol.* **2008**, *63* (1), 156–162.
- 411 (15) Zhu, L.; Chen, B.; Tao, S.; Chiou, C. T. Interactions of organic contaminants with  
412 mineral-adsorbed surfactants. *Environ. Sci. Technol.* **2003**, *37* (17), 4001–4006.

- 413 (16) Chen, B. L.; Zhu, L. Z.; Zhu, J. X. Configurations of the bentonite-sorbed myristylpyridinium  
414 cation and their influences on the uptake of organic compounds. *Environ. Sci. Technol.* **2005**, *39*  
415 (16), 6093–6100.
- 416 (17) Zhu, J.; Zhu, L.; Zhu, R.; Chen, B. Microstructure of organo-bentonites in water and the  
417 effect of steric hindrance on the uptake of organic compounds. *Clays Clay Miner.* **2008**, *56* (2),  
418 144–154.
- 419 (18) Bartelt-Hunt, S. L.; Burns, S. E.; Smith, J. A. Nonionic organic solute sorption onto two  
420 organobentonites as a function of organic-carbon content. *J. Colloid Interface Sci.* **2003**, *266* (2),  
421 251–258.
- 422 (19) Xu, L.; Zhu, L. Structures of OTMA- and DODMA-bentonite and their sorption  
423 characteristics towards organic compounds. *J. Colloid Interface Sci.* **2009**, *331* (1), 8–14.
- 424 (20) Xu, L.; Zhang, M.; Zhu, L. Adsorption-desorption behavior of naphthalene onto CDMBA  
425 modified bentonite: Contribution of the pi-pi interaction. *Appl. Clay Sci.* **2014**, *100*, 29–34.
- 426 (21) Nguyen, V. N.; Nguyen, T. D. C.; Dao, T. P.; Tran, H. T.; Nguyen, D. B.; Ahn, D. H. Synthesis  
427 of organoclays and their application for the adsorption of phenolic compounds from aqueous  
428 solution. *J. Ind. Eng. Chem.* **2013**, *19* (2), 640–644.
- 429 (22) Bonczek, J. L.; Harris, W. G.; Nkedi-Kizza, P. Monolayer to bilayer transitional arrangements  
430 of hexadecyltrimethylammonium cations on Na-montmorillonite. *Clays Clay Miner.* **2002**, *50* (1),  
431 11–17.
- 432 (23) Greathouse, J. A.; Cygan, R. T. Water structure and aqueous uranyl(VI) adsorption equilibria  
433 onto external surfaces of beidellite, montmorillonite, and pyrophyllite: Results from molecular  
434 simulations. *Environ. Sci. Technol.* **2006**, *40* (12), 3865–3871.
- 435 (24) Cygan, R. T.; Greathouse, J. A.; Heinz, H.; Kalinichev, A. G. Molecular models and  
436 simulations of layered materials. *J. Mater. Chem.* **2009**, *19* (17), 2470–2481.
- 437 (25) Greathouse, J. A. and Cygan, R. T. Molecular simulation of clay minerals. In *Handbook of*  
438 *Clay Science*, 2<sup>nd</sup> ed.; Bergaya, F., Lagaly, G., Eds.; Elsevier: Amsterdam 2013; pp 405–424.
- 439 (26) Morrow, C. P.; Yazaydin, A. O.; Krishnan, M.; Bowers, G. M.; Kalinichev, A. G.; Kirkpatrick,  
440 R. J. Structure, Energetics, and Dynamics of Smectite Clay Interlayer Hydration: Molecular  
441 Dynamics and Metadynamics Investigation of Na-Hectorite. *J. Phys. Chem. C* **2013**, *117* (10),  
442 5172–5187.
- 443 (27) Zhang, L.; Lu, X.; Liu, X.; Zhou, J.; Zhou, H. Hydration and Mobility of Interlayer Ions of  
444 (Nax, Cay)-Montmorillonite: A Molecular Dynamics Study. *J. Phys. Chem. C* **2014**, *118* (51),  
445 29811–29821.
- 446 (28) Zhou, Q.; Shen, W.; Zhu, J.; Zhu, R.; He, H.; Zhou, J.; Yuan, P. Structure and dynamic  
447 properties of water saturated CTMA-montmorillonite: molecular dynamics simulations. *Appl.*  
448 *Clay Sci.* **2014**, *97–98*, 62–71.
- 449 (29) Zhou, J.; Lu, X.; Zhu, J.; Liu, X.; Wei, J.; Zhou, Q.; Yuan, P.; He, H. Interlayer structure and  
450 dynamics of HDTMA(+)-intercalated rectorite with and without water: a molecular dynamics  
451 study. *J. Phys. Chem. C* **2012**, *116* (24), 13071–13078.
- 452 (30) Zhu, R.; Chen, W.; Shapley, T. V.; Molinari, M.; Ge, F.; Parker, S. C. Sorptive characteristics  
453 of organomontmorillonite toward organic compounds: a combined DFT and molecular dynamics  
454 simulation study. *Environ. Sci. Technol.* **2011**, *45* (15), 6504–6510.
- 455 (31) Zhu, R.; Hu, W.; You, Z.; Ge, F.; Tian, K. Molecular dynamics simulation of TCDD  
456 adsorption on organo-montmorillonite. *J. Colloid Interface Sci.* **2012**, *377*, 328–333.

- 457 (32) Zhao, Q.; Burns, S. E. Molecular dynamics simulation of secondary sorption behavior of  
458 montmorillonite modified by single chain quaternary ammonium cations. *Environ. Sci. Technol.*  
459 **2012**, *46* (7), 3999–4007.
- 460 (33) Zhao, Q.; Burns, S. E. Modeling sorption and diffusion of organic sorbate in  
461 hexadecyltrimethylammonium-modified clay nanopores - a molecular dynamics simulation study.  
462 *Environ. Sci. Technol.* **2013**, *47* (6), 2769–2776.
- 463 (34) Shapley, T. V.; Molinari, M.; Zhu, R.; Parker, S. C. Atomistic modeling of the sorption free  
464 energy of dioxins at clay-water interfaces. *J. Phys. Chem. C* **2013**, *117* (47), 24975–24984.
- 465 (35) Loewenstein, W. The distribution of aluminum in the tetrahedra of silicates and aluminates.  
466 *Am. Mineral.* **1954**, *39* (1–2), 92–96.
- 467 (36) Smith, W.; Forester, T. DL\_POLY\_2. 0: A general-purpose parallel molecular dynamics  
468 simulation package. *J. Mol. Graph.* **1996**, *14* (3), 136–141.
- 469 (37) Cygan, R. T.; Liang, J. J.; Kalinichev, A. G. Molecular models of hydroxide, oxyhydroxide,  
470 and clay phases and the development of a general force field. *J. Phys. Chem. B* **2004**, *108* (4),  
471 1255–1266.
- 472 (38) Berendsen, H.; Postma, J.; van Gunsteren, W.; Hermans, J., Interaction models for water in  
473 relation to protein hydration. In *Intermolecular Forces*; Pullman, B., Ed.; Reidel: Dordrecht 1981;  
474 p 331–342.
- 475 (39) Dauberosguthorpe, P.; Roberts, V. A.; Osguthorpe, D. J.; Wolff, J.; Genest, M.; Hagler, A. T.  
476 Structure and energetics of ligand-binding to proteins - escherichia-coli dihydrofolate reductase  
477 trimethoprim, a drug-receptor system. *Proteins: Struct., Funct., Genet.* **1988**, *4* (1), 31–47.
- 478 (40) Crabtree, J. C.; Molinari, M.; Parker, S. C.; Purton, J. A. Simulation of the Adsorption and  
479 Transport of CO<sub>2</sub> on Faujasite Surfaces. *J. Phys. Chem. C* **2013**, *117* (42), 21778–21787.
- 480 (41) Martins, D. M. S.; Molinari, M.; Goncalves, M. A.; Mirao, J. P.; Parker, S. C. Toward  
481 Modeling Clay Mineral Nanoparticles: The Edge Surfaces of Pyrophyllite and Their Interaction  
482 with Water. *J. Phys. Chem. C* **2014**, *118* (47), 27308–27317.
- 483 (42) Guardia, E.; Marti, J.; Garcia-Tarres, L.; Laria, D. A molecular dynamics simulation study of  
484 hydrogen bonding in aqueous ionic solutions. *J. Mol. Liq.* **2005**, *117* (1–3), 63–67.
- 485 (43) Wang, J.; Kalinichev, A. G.; Kirkpatrick, R. J. Effects of substrate structure and composition  
486 on the structure, dynamics, and energetics of water at mineral surfaces: A molecular dynamics  
487 modeling study. *Geochim. Cosmochim. Acta* **2006**, *70* (3), 562–582.
- 488 (44) Wang, J.; Kalinichev, A. G.; Kirkpatrick, R. J.; Cygan, R. T. Structure, energetics, and  
489 dynamics of water adsorbed on the muscovite (001) surface: A molecular dynamics simulation. *J.*  
490 *Phys. Chem. B* **2005**, *109* (33), 15893–15905.
- 491 (45) Ngouana W, B. F.; Kalinichev, A. G. Structural arrangements of isomorphic substitutions in  
492 smectites: molecular simulation of the swelling properties, inter layer structure, and dynamics of  
493 hydrated cs-montmorillonite revisited with new clay models. *J. Phys. Chem. C* **2014**, *118* (24),  
494 12758–12773.
- 495 (46) Marry, V.; Rotenberg, B.; Turq, P. Structure and dynamics of water at a clay surface from  
496 molecular dynamics simulation. *Physical Chemistry Chemical Physics* **2008**, *10* (32), 4802–4813.
- 497 (47) Abraham, M. H.; Chadha, H. S.; Leitao, A. R. E.; Mitchell, R. C.; Lambert, W. J.; Kaliszan,  
498 R.; Nasal, A.; Haber, P. Determination of solute lipophilicity, as log P(octanol) and log P(alkane)  
499 using poly(styrene-divinylbenzene) and immobilised artificial membrane stationary phases in  
500 reversed-phase high-performance liquid chromatography. *J. Chromatogr. A* **1997**, *766* (1–2),

- 501 35–47.
- 502 (48) Liu, X.; Zhu, R.; Ma, J.; Ge, F.; Xu, Y.; Liu, Y. Molecular dynamics simulation study of  
503 benzene adsorption to montmorillonite: Influence of the hydration status. *Colloids Surface, A*.  
504 **2013**, *434*, 200-206.
- 505 (49) Aggarwal, V.; Li, H.; Boyd, S. A.; Teppen, B. J. Enhanced sorption of trichloroethene by  
506 smectite clay exchanged with Cs<sup>+</sup>. *Environ. Sci. Technol.* **2006**, *40* (3), 894-899.
- 507 (50) Chappell, M. A.; Laird, D. A.; Thompson, M. L.; Li, H.; Teppen, B. J.; Aggarwal, V.;  
508 Johnston, C. T.; Boyd, S. A. Influence of smectite hydration and swelling on atrazine sorption  
509 behavior. *Environ. Sci. Technol.* **2005**, *39* (9), 3150-3156.
- 510 (51) Barrett, J., *Inorganic Chemistry in Aqueous Solution*. Royal Society of Chemistry: Cambridge,  
511 2003.
- 512 (52) Zhu, R.; Zhu, L. Thermodynamics of naphthalene sorption to organoclays: Role of surfactant  
513 packing density. *J. Colloid Interface Sci.* **2008**, *322* (1), 27–32.
- 514 (53) Zhu, R.; Chen, W.; Liu, Y.; Zhu, J.; Ge, F.; He, H. Application of linear free energy  
515 relationships to characterizing the sorptive characteristics of organic contaminants on organoclays  
516 from water. *J. Hazard. Mater.* **2012**, *233*, 228–234.
- 517 (54) Endo, S.; Goss, K.-U. Applications of Polyparameter Linear Free Energy Relationships in  
518 Environmental Chemistry. *Environ. Sci. Technol.* **2014**, *48* (21), 12477–12491.
- 519 (55) Nguyen, T. H.; Goss, K. U.; Ball, W. P. Polyparameter linear free energy relationships for  
520 estimating the equilibrium partition of organic compounds between water and the natural organic  
521 matter in soils and sediments. *Environ. Sci. Technol.* **2005**, *39* (4), 913–924.
- 522 (56) Vitha, M.; Carr, P. W. The chemical interpretation and practice of linear solvation energy  
523 relationships in chromatography. *J. Chromatogr. A* **2006**, *1126* (1–2), 143–194.
- 524
- 525
- 526



Fig. 1 Snapshots (left graph), 2D density profiles (middle graph), and Z-density profiles (right graph) of hydrated CTMA-Mt with different loading level: (a) 0.33 CEC; (b) 1.00 CEC; (c) 1.66 CEC. In the snapshots: gray ball, C3 (CTMA C on alkyl chains); blue ball, N3 (CTMA N); white ball, H3 (CTMA H); green stick, phenol; purple ball, Ca ion; red line, water. In the 2D density profiles: C3 in yellow; CR in blue. In the Z-density profiles: N3 in blue; C3 in dark gray; CR in green; OW (water O) in red; HW (water H) in black;  $\text{Ca}^{2+}$  in purple;  $\text{Br}^-$  in brown.

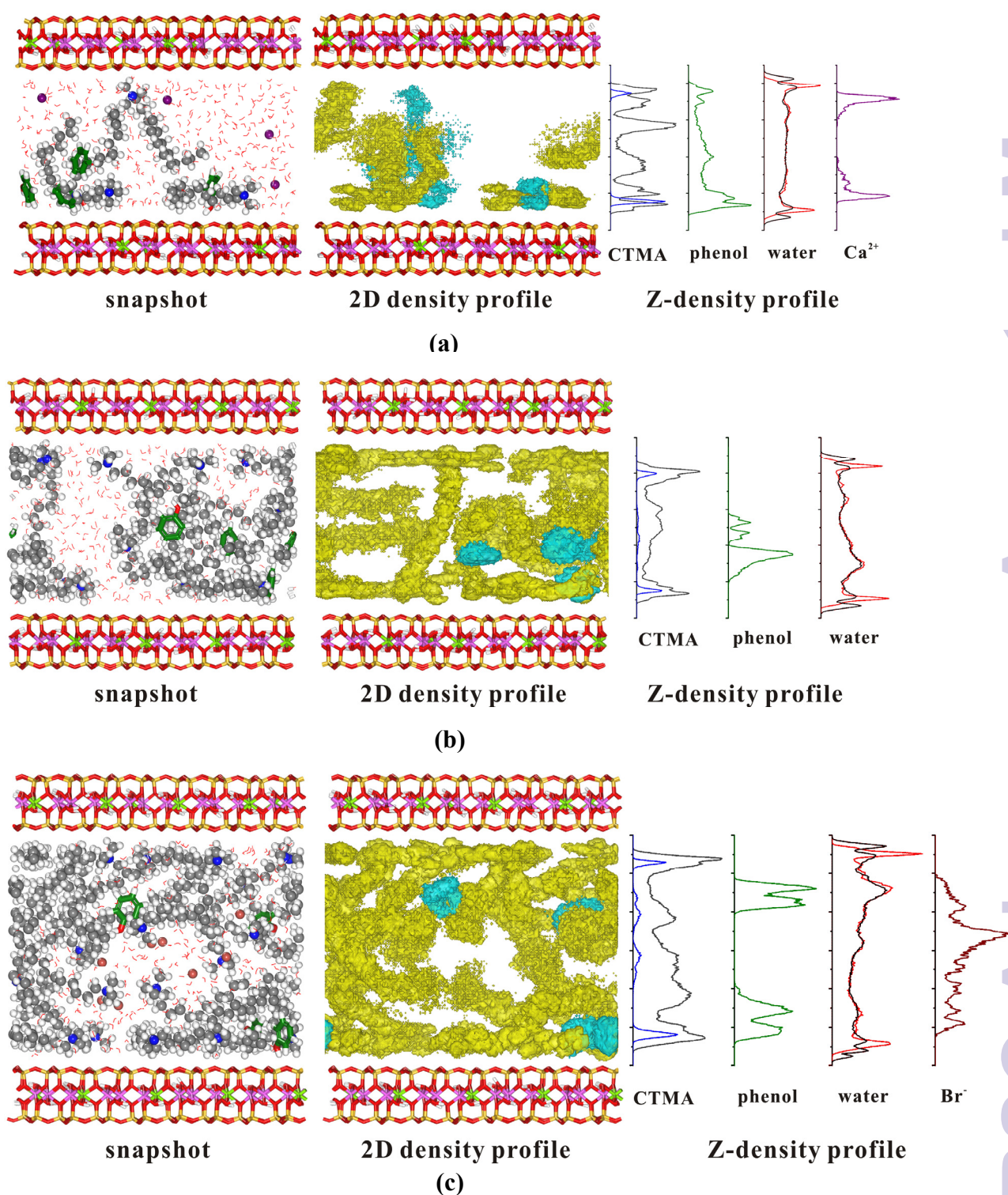


Fig. 2 RDF profiles of the hydrated CTMA-Mt. (a) Ca-OW and Ca-HC for 0.33CTMA-Mt; (b) Br-HW, Br-HC, and Br-N3 for 1.66CTMA-Mt.

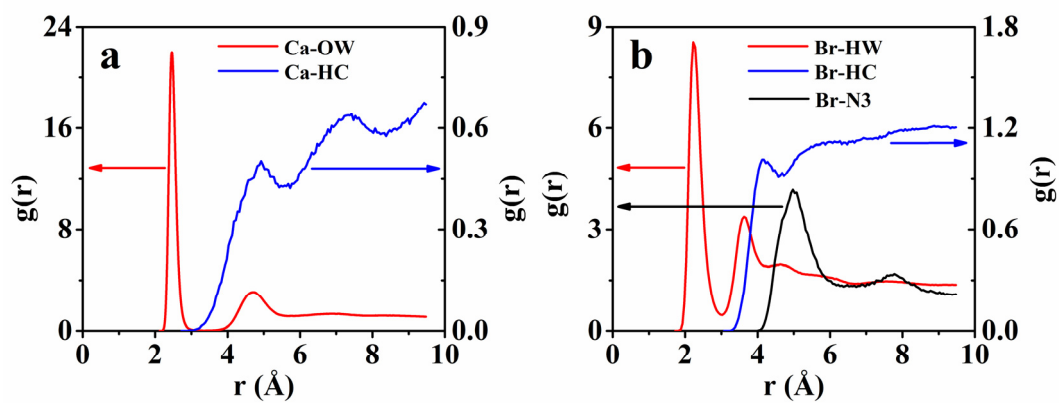


Fig. 3 RDF profiles of the hydrated CTMA-Mt. (a) Ca-OW and Ca-HW for 0.33CTMA-Mt; (b) Br-OW and Br-HW for 1.66CTMA-Mt; (c) Ca-OP (phenol O) and Ca-HP (phenol H) for 0.33CTMA-Mt; (d) Br-OP and Br-HP for 1.66CTMA-Mt.

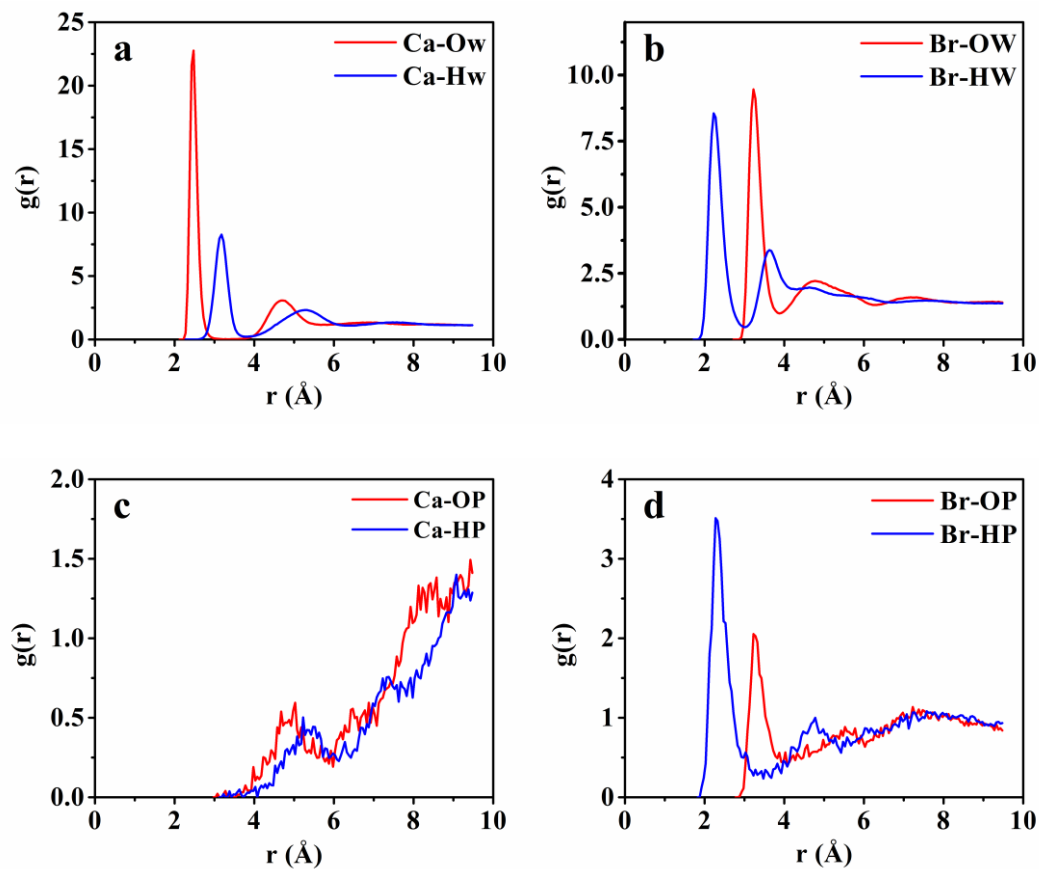




Fig. 4 H-bond network within CTMA-Mt interlayer (CTMA molecules were removed for better view). H-bond formed between water and phenol near  $\text{Ca}^{2+}$  or  $\text{Br}^-$  ions were particularly shown. (a) 0.33CTMA-Mt; (b) 1.66CTMA-Mt.

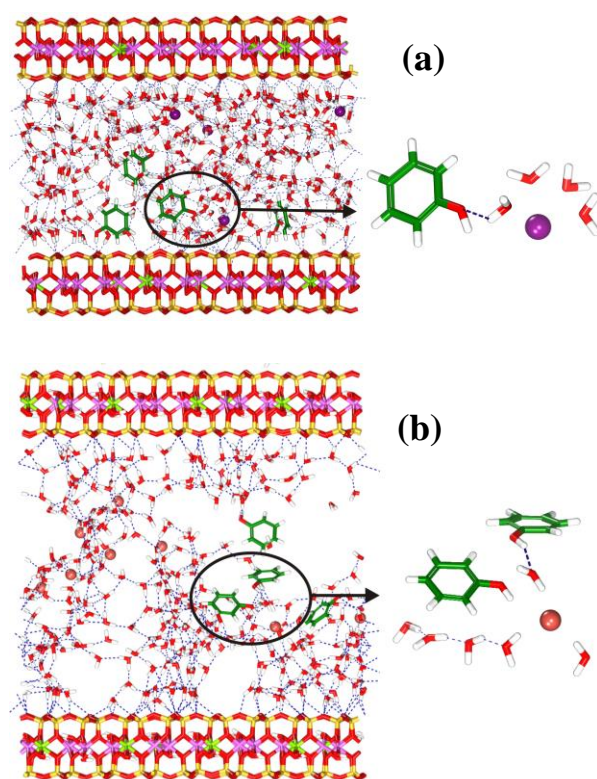


Table 1 Average H-bond numbers formed for each phenol molecule (with water molecules), the self-diffusion coefficients of C3 ( $D_{C3}$ ) and CP ( $D_{CP}$ ), and CTMA packing density ( $d_{CTMA}$ ).  $N_D$ : H-bond numbers in the case phenol as proton donor;  $N_A$ : H-bond numbers in the case phenol as proton acceptor;  $N_{total}$ : total H-bond numbers for each phenol ( $N_D + N_A$ ).

sample	average H-bond number				$D_{C3}$ ( $10^{-11}$ m <sup>2</sup> /s)	$D_{CP}$ ( $10^{-11}$ m <sup>2</sup> /s)	$d_{CTMA}$ (g/cm <sup>3</sup> )
	$N_D$	$N_A$	$N_{total}$	$N_D/N_A$			
0.33CTMA-Mt	0.280	0.143	0.423	1.96	3.2	4.9	0.602
1.0CTMA-Mt	0.283	0.105	0.388	2.69	2.3	1.9	0.764
1.66CTMA-Mt	0.271	0.064	0.335	4.25	1.7	2.0	0.898